Journal of Natural Disaster Science, Volume 24, Number 1, 2002, pp1-13

Determination of Subsurface Structure of Tottori Plain Using Microtremors and Gravity Anomaly

Tatsuya NOGUCHI and Ryohei NISHIDA
Department of Civil Engineering, Tottori University
(Received for 3. Apr., 2002)

ABSTRACT

Microtremor observations and a gravity survey were made to determine the subsurface structures of the Tottori Plain. This area was severely damaged during the 1943 Tottori earthquake (M7.2), damage being concentrated in the plain. Microtremors were recorded by seismic arrays (8 sites) and 3-component single-site observation (417 points). Gravity data were obtained at about 400 points. The microtremor data were analyzed by the spatial auto correlation (SPAC) method and the horizontal-to-vertical spectral ratio (H/V). The subsurface structures were determined by 1) S-wave velocity structure models obtained at the array observation sites, 2) a 3D bedrock configuration based on H/V and the residual gravity anomaly, 3) 2D density structures for three cross sections obtained using the gravity anomaly based on a depths of S-wave velocity structures. A shallow bedrock area extends over a belt-like zone along the coast. This bedrock suddenly deepens from the eastern mountainous area to the plain. The depth to the Vs=3500m/s layer ranges from a 300m minimum to an 800m maximum.

1. INTRODUCTION

The Tottori plain in the Sanin area of Japan, the target area of this study, was severely damaged by the 1943 Tottori earthquake (M7.2). The severely damaged area was concentrated on the Tottori plain (Architectural Institute of Japan, 1944), whereas there was less damage in the western and southern parts of Tottori City. This concentration of damage is thought to have been caused by the characteristics of the earthquake ground motion affected by the local subsurface structure of the Tottori plain.

The subsurface cross section (Tottori Subsurface Institutes, 1991) for which borehole data on the sedimentary layer had been collected was investigated. A contour map (Akagi et al., 1993) of the bedrock of the diluvium and alluvium had already been obtained. In addition, PS logging (exploration of the sedimentary layer) and elastic wave exploration of the mountainous area (e.g., Oyo corporation, 1996) has been done. At several points in the rock layer structure beneath the plain (stratum of Neogene system or Paleogene system), gravity anomal was found by a gravity survey. No detailed density structure however has been determined and PS logging and elastic wave exploration have been done only on limited points.

There are two ways to determine subsurface structures. One is to visually explore the geologic profile by means of bore-hole data The other is to make a geophysical exploration to obtain physical parameters such as elastic wave velocity and investigating density. Effective methods for obtaining elastic wave velocity and 2D or 3D bedrock structures are microtremor exploration and a gravity survey. The use of microtremors is divisible into three types: array observation using several seismometers, 3-component observation at a single site (single-site observation), and 3-component observation at soil and rock sites. Array observation records are analyzed by the spatial auto correlation (SPAC) or F-K method. The S-wave velocity structure can be determined from array records by these methods. Single-site observation records can be analyzed by means of the horizontal-to-vertical spectral ratio (H/V). Soil and rock site observation records can be analyzed by means of the horizontal- (soil site) - to - horizontal (rock site) spectral ratio.

Array observations have been made at many sites in order to determine the S-wave structure to a depth of 2 or 3km. (e.g., Okada et al., 1990; Yamanaka et al., 1995; Miyakoshi et al., 1994; Matsushima et al., 1990). The predominant period of the surface layers and depth to the bedrock have been determined at several sites by a H/V (e.g., Ohmachi et al., 1994; Tokimatsu et al., 1997; Ishida et al., 1996). Gravity exploration can determine a density structure by use of Bouguer gravity anomaly. The 3D configuration of bedrock from several meters to several kilometers and a density structure model have been obtained by this method (e.g., Kikuchi, 1982; Komazawa, 1984; Makino, 1997). In those explorations, the subsurface structures were determined on the basis of data being in the same period band as that of the estimation of strong motion by means of the elastic wave theory. Microtremor exploration and gravity observations therefore are applicable for determining the subsurface structure in this the Tottori plain area.

The purpose of our study was to determine the subsurface structures of the Tottori plain by the use of microtremors and gravity observation records.

2. GEOLOGICAL FEATURES

The topography (Akagi et al.,1993) of the Tottori plain is that

KEY WORDS: subsurface structure, Tottori plain, microtremors, Bouguer gravity anomaly

of sand dunes expanding along the coast, a delta area that occupies the main part of the plain, an alluvial fan in the southern part of the plain , and a valley plain. In the north, there is an extensive coastal sand dune, and Mt. Kyushou is located southeast of Tottori City.

A geological map is shown in Figure 1. The Cretaceous - Cenozoic stratigraphy is shown in Table 1. The surface rocks are comprised of the Tertiary system, and the Mesozoic volcanic granite rocks (Akagi et al., 1993). The Mesozoic volcanic are distributed in the southern of Mt. Kyushou on the southwest edge of the plain. The granite rocks occur along the south edge of Koyama Pond, in the main part of Mt. Kyushou and in the mountainous area that stretches northwest from Mt. Kyushou. The Neogene system stratum is composed pyroclastic and sedimentary rocks. Pyroclastic rocks that consist of tuff and basalt are distributed along the southern edge of Koyama Pond and in the southwest of the plain. Conglomerate and sandstone are widely distributed in the southern part of the plain and mudstone occurs in the southeast.

Table 1. Quaternary stratigraphy of the Tottori plain (Akagi et al., 1993).

Geological Age		Stratigraphy	
Cenozoic	Quaternary	Alluvium	Modern Dune
			Fluvial Deposits, Lagoonal and Lacustrine Deposits
			Alluvium, Talus
		Diluvium	Volcanic Ash
			Ancient Dune Sand
			Terrace Deposits
			Mud
	Neogene		Mudstone Member
			Conglomerate Sandstone
			Pyroclastic Member
	Paleogene	Granite	
Mesozoic	Cretaceous	Mesozoic Volcanic Rocks	

3. OBSERVATION

3.1 Microtremor observations

Array observations at 8 sites and 3-component single-site observations at 410 points were made to observe microtremors in the Tottori plain. Locations of the observation points are shown in Figure 2 and the observation system in Figure 3. Observations were made at 417 points at night from October 1998 to October 2001. The array observation system consisted of four vertical seismometers, a direct current amplifier, and a data-recorder. Here, the array with a 3 - 70m radius is called the S-array and that with a 200 - 500m radius the L-array. Natural periods (T_0) of the seismometers were 1s for the S-arrays and 8s for the L-arrays. An overview of array observations is given in Table 2. A 3-compo-

Table 2. Overview of the observation system and setting. A: Simultaneous observation system using a cable, seismometer of T_0=1s, for the S-array. B: System using a GPS timing receiver, seismometer of T_0=8s, for the L-array.

Site	System	Radius (m)	Sampling Frequency (Hz)	Amplifier Gain
TTD	A	250, 500	100	1000
	B	3, 10, 30, 50		
YNG	A	250, 500		500 (250m) 1000 (other)
	B	3, 10, 30, 50, 60		
JHK	A	250, 500		1000
	B	3, 10, 30, 60		
KAR	A	250, 500		
	B	3, 10, 30, 70		
SHB	A	250		
	B	3, 10, 30, 50		
GNT	A	250		
	B	3, 10, 30, 70		
NIK	A	125,250		
	B	10,30	500	
TTA	A	250, 500	100	
	B	10, 30, 60	500	

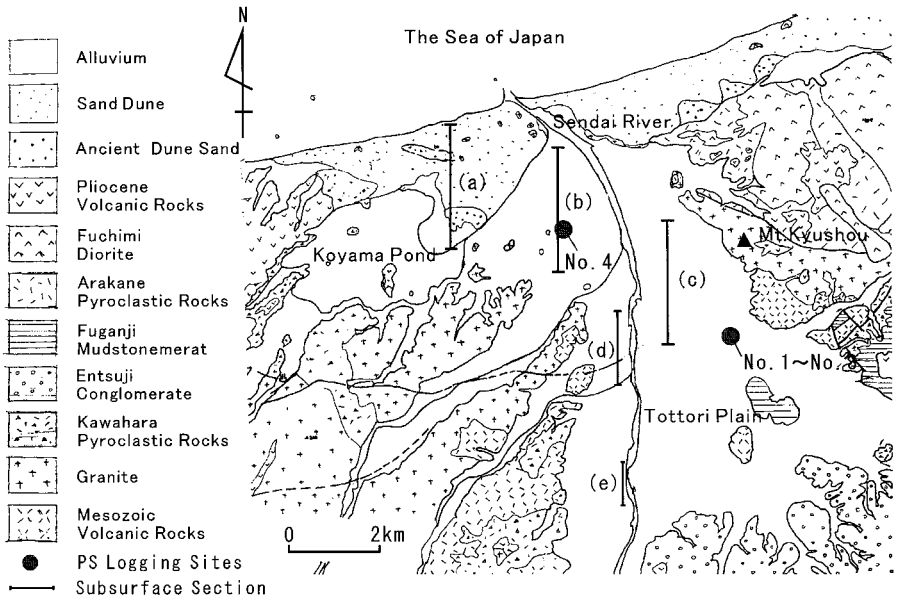

Fig. 1 Geological map of the Tottori plain (Akagi et al., 1993). ●: PS logging sites. Line segments represent the subsurface sections in Figure 5.

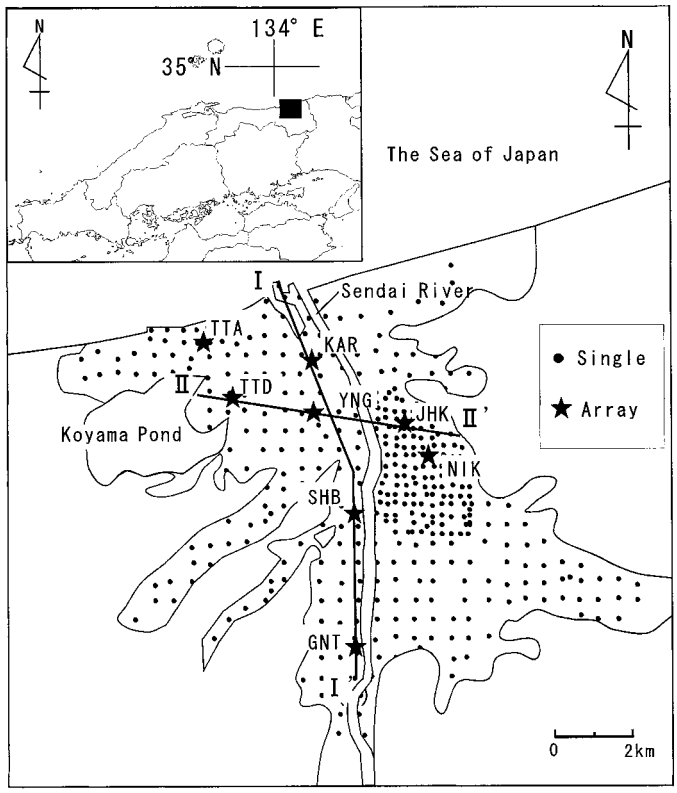

Fig. 2 Locations of microtremor observation sites. Dots: single-site observation sites, and stars: array observation sites.

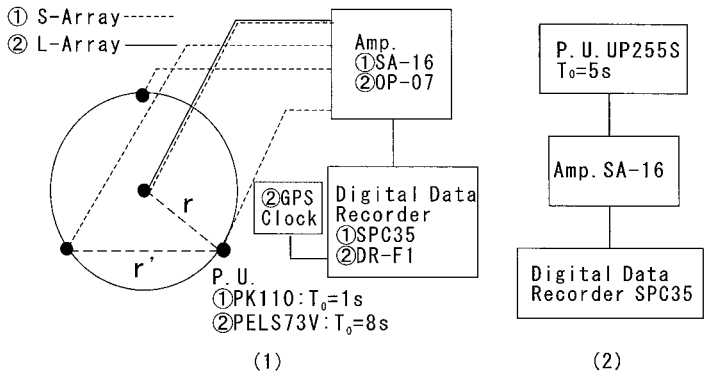

Fig. 3 Array observation system (1); S-array system ①, L-array system ②. Single-site observation system (2).

nent seismometer (T_0=5s) was used in the single site observation system.

3.2 Gravity observations

This information was used in the gravity analysis. ① 417 points at 500 m interval (Nishida et al., 2001), ② 197 points at 200 - 300m intervals in central Tottori City (Nakagawa et. al., 1993), ③ 192 points at 50 - 200m intervals in the Yoshioka hot spring area (Tottori Prefecture, 1999), ④ 43 points in the mountainous area surrounding the plain (Komazawa et al., 2000), ⑤ 296 points around the Yoshioka - Shikano fault area and its peripheral mountains. A Racoste Lon Berg's G type gravimeter was used. The precision of the elevation measurements was kept within 1m.

4. ANALYSIS

4.1 Analysis of microtremor data

Portions of 40.96s or 81.92s without artificial noise were selected from the array observation records. The dispersion curve of the phase velocity was calculated by the SPAC method (Aki, 1957). Spectra were smoothed by use of a Parzen window with a 0.3Hz band for the S-array and a 0.1Hz one for the L-array. Dispersion curves for the phase velocity are shown in Figure 4. A dispersion curve was obtained for each array radius (dots) and the theoretical curve (solid line) was obtained for the final model.

Portions of 20.48s without artificial noise were selected from the 3-component microtremor records. H/V was calculated by use

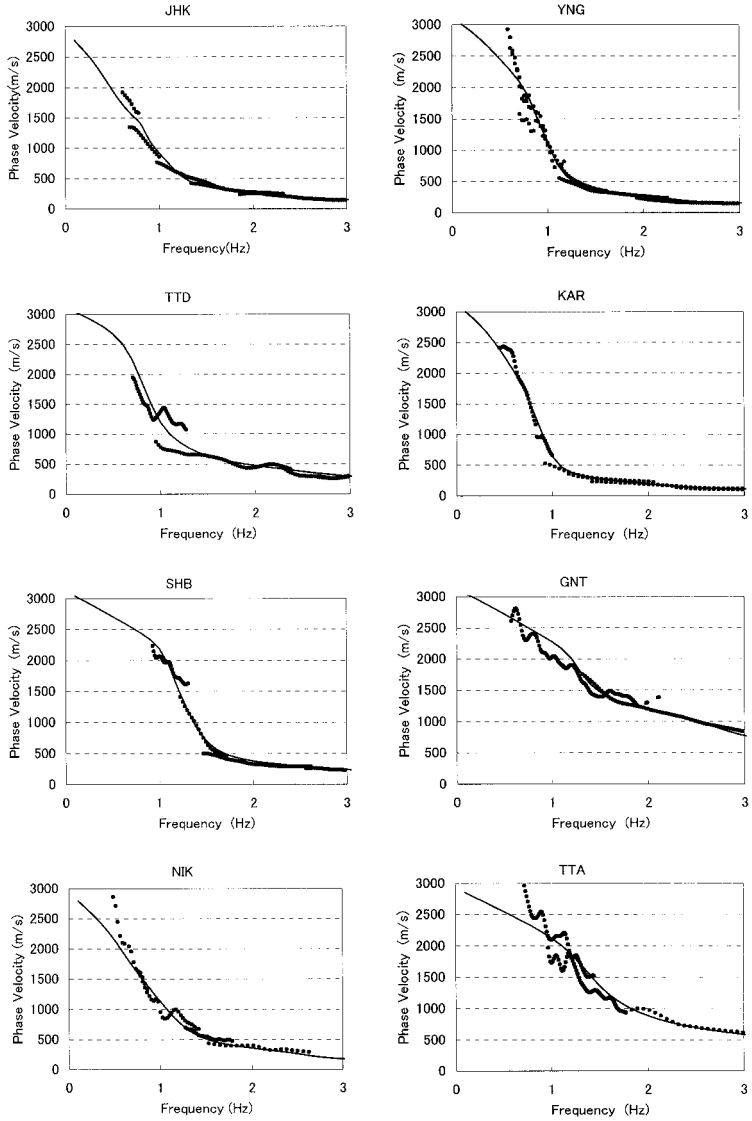

Fig. 4 Phase velocity dispersion curves at array observation sites. Dots show the phase velocity, solid lines the theoretical curves obtained from the final subsurface structure model.

of using the averaged Fourier spectra of the selected data. Horizontal components were composed. Spectra were smoothed by means of a Parzen window with a 0.3Hz band .

4.2 Analysis of gravity data

Terrain correction was made with a topographic 50m mesh digital data for ①,②,③,⑤ data and a 250m mesh for ④ to obtain the Bouguer gravity anomaly. Density measurement results for rock samples (NEDO, 1977) and CVUR method (Komazawa, 1995) were used to determine a suitable density, and an automatic 2D analysis method (Komazawa, 1995) to determine a 2D density structure. This method uses the automatic forwarding methods of Talwani et al. (1959). The parameters required are density differences between surface and bedrock layers of two homogeneous layers and a control point for bedrock depth.

5. DETERMINATION OF THE SUBSURFACE STRUCTURE

5.1 Determination of the S-wave velocity structure

The parameters (number of layers, density, P-wave velocity; [Vp] S-wave velocity; [Vs]) used in the subsurface structure models were selected on the basis of the geological features and subsurface cross section (Tottori Subsurface Institute, 1991). Density was obtained by referring to a previous report (Society of Exploration Geophysicists of Japan, 1988), and Vp was found by the formula (Kitsunezaki et al., 1990),

$$Vp = 1.11Vs + 1290 \ (m/s) \qquad (1)$$

To obtain the parameters of the sedimentary layers, a subsurface cross section (Figure 5) (Tottori Subsurface Institute, 1991) around the array observation points and PS logging results for the

Table 3. PS Logging profiles (Oyo Corporation, 1996). Location of these points are shown in Figure 1.

(1) No.1

Depth (m)	Facies	Vp (m/s)	Vs (m/s)
0～6	Sand and gravel with small stones, clay	1000	94
6～10	Clay, humus soil, small grains		150
10～11	Sand and gravel with small stones		350
11～21	Sandy silt with gravel etc.	2000	
21～24	Sand and gravel with small stones		550

(2) No.2

Depth (m)	Facies	Vp (m/s)	Vs (m/s)
0～4	Sand and gravel with small stones	800	90
4～5	Clay		150
5～7	Clay, small grains	1800	250
7～13	Sand and gravel		
13～21	Sand and gravel with clay		500

(3) No.3

Depth (m)	Facies	Vp (m/s)	Vs (m/s)
0～2	Artificial	900	140
2～7	Clay	1500	120
7～13	Silty sand		160
13～18	Clay		140
18～30	Sand and gravel	1800	480

(4) No.4

Depth (m)	Facies	Vp (m/s)	Vs (m/s)
0～6	clay	430	80
6～13	sand	1000	160
13～26	clay		140
26～36	sandy silt	1500	200
36～40	sand and gravel	2100	480

locations shown in Figure 1 (Table 3) (Oyo Corporation, 1996) were used. The velocity of the uppermost layer was decided such that it fits the minimum phase velocity of the observation value.

From the geological background, the rock layer is thought to be divided mainly into granite rock of the Neogene, and Paleogene systems and Mesozoic Volcanic rocks (Table 1). The Tottori Green Tuff Research Group (1989) reported that the Neogene system stratum does not have clear boundaries and is an unconformity. Accordingly, the velocity value is considered to increase gradually in the deep part of the layer. We further divide the Neogene system into three strata based on the degree of consolidation; ① slight consolidation, ② medium consolidation and ③ marked consolidation layers. Moreover to determine the velocity of layers we assumed that the ④ granite of the Paleogene or Mesozoic Volcanic rock layer is the lowest stratum. In the rock layer, the velocity contrast is greatest at the boundary between layers ③ and ④. For

Table 4. Parameters for determination of the S-wave velocity structural model.

Density (g/cm^3)	Vp (m/s)	Vs (m/s)	Geological Age	Geology
1.6	1400	100	Quaternary	Alluvium & Diluvium
	1460	150		
1.7	1510	200		
1.8	1730	300		
2.0	1840	500		
2.1	2060	700	Neogene	small consolidation
2.2	2390	1000		middle consolidation
2.4	2940	1500		large consolidation
2.6	5180	3500	Paleogene & Cretaceous	Granite, Mesozoic Volcanic Rocks

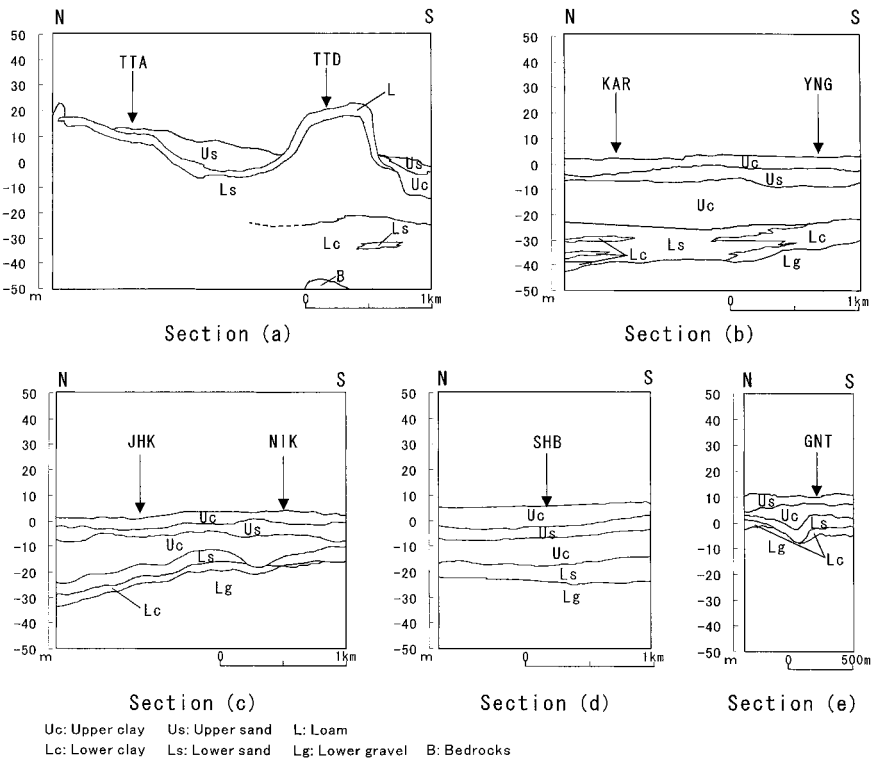

Fig. 5 Subsurface cross sections around the array observation. Locations of sections are shown in figure 1 (Tottori Subsurface Institute, 1991).

S-wave velocity values of the layers assumed from the geological classification, ① Vs=700m/s, ② 1000m/s, ③ 1500m/s, ④ 3500m/s were determined using experiential values (Miyakoshi, 1994). Parameters of the subsurface structure models are shown in Table 4.

By restricting Vs and Vp densities to the given value and changing only the layer thickness, a subsurface model could be established by trial and error. The final subsurface structure was obtained by these processes (Table 5).

Based on the I-I' section in the north to south direction and the II-II' section in the east to west direction , columnar sections of the S-wave velocity structures at 7 observation sites are shown in Figure 6. Minimum and maximum depths to the Vs=3500m/s layer respectively of about 300m and 800m were obtained. In the I-I' section, the tendency is to gradually become deeper from GNT to KAR and suddenly to become shallow at TTA. In the II-II' section, the trend is to deepen from TTD on the west to JHK.

Table 5. Final subsurface structure models at the array observation sites.

(1) TTD site model

ρ(g/cm³)	Vp(m/s)	Vs(m/s)	Thickness(m)
1.6	1455	150	17
1.8	1620	300	35
2.0	1840	500	40
2.1	2060	700	50
2.2	2390	1000	70
2.4	2940	1500	250
2.6	5180	3500	∞

(2) YNG site model

ρ(g/cm³)	Vp(m/s)	Vs(m/s)	Thickness(m)
1.6	1400	100	10
1.6	1455	150	22
2.0	1840	500	20
2.1	2060	700	120
2.2	2390	1000	200
2.4	2940	1500	300
2.6	5180	3500	∞

(3) JHK site model

ρ(g/cm³)	Vp(m/s)	Vs(m/s)	Thickness(m)
1.6	1400	100	10
1.6	1455	150	20
2.0	1840	500	25
2.1	2060	700	160
2.2	2390	1000	230
2.4	2940	1500	350
2.6	5180	3500	∞

(4) TTA site model

ρ(g/cm³)	Vp(m/s)	Vs(m/s)	Thickness(m)
1.7	1510	200	9
1.8	1620	300	25
2.0	1840	500	20
2.1	2060	700	30
2.2	2390	1000	80
2.4	2940	1500	240
2.6	5180	3500	∞

(5) SHB site model

ρ(g/cm³)	Vp(m/s)	Vs(m/s)	Thickness(m)
1.6	1400	100	5
1.6	1455	150	20
2.0	1840	500	20
2.1	2060	700	70
2.2	2390	1000	80
2.4	2940	1500	150
2.6	5180	3500	∞

(6) KAR site model

ρ(g/cm³)	Vp(m/s)	Vs(m/s)	Thickness(m)
1.6	1400	100	10
1.6	1455	150	30
2.0	1840	500	25
2.1	2060	700	150
2.2	2390	1000	200
2.4	2940	1500	300
2.6	5180	3500	∞

(7) GNT site model

ρ(g/cm³)	Vp(m/s)	Vs(m/s)	Thickness(m)
1.7	1510	200	10
2.0	1840	500	15
2.1	2060	700	70
2.2	2390	1000	100
2.4	2940	1500	100
2.6	5180	3500	∞

(8) NIK site model

ρ(g/cm³)	Vp(m/s)	Vs(m/s)	Thickness(m)
1.6	1455	150	28
2.0	1840	500	50
2.1	2060	700	110
2.2	2390	1000	170
2.4	2940	1500	320
2.6	4590	3000	∞

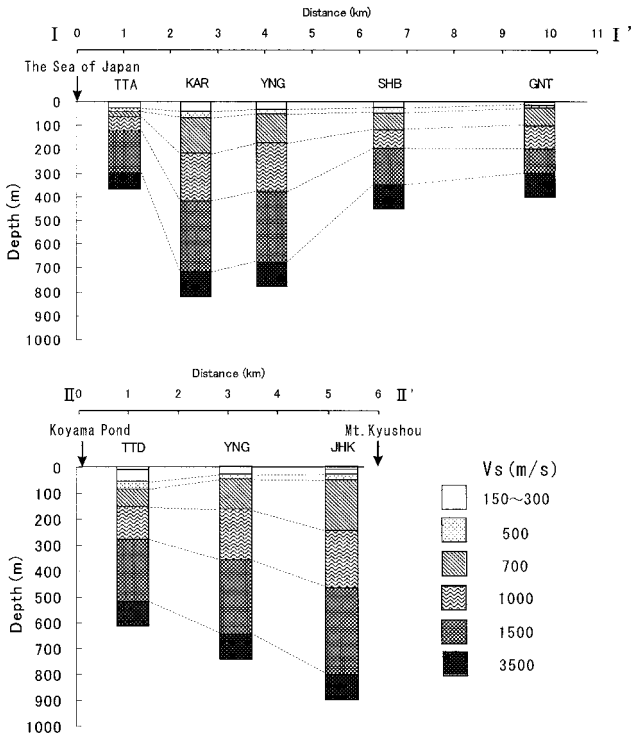

Fig. 6 Density measurements of rock samples, collected in the mountainous area of the eastern region (NEDO, 1977).

5.2 Bedrock structure determined by H/V

We tried to determined bedrock depth from the peak period of the observed microtremors, H/V, at the central array point. To determine bedrock depth, the bedrock layer that responds to the H/V peak period must be ascertained. Rayleigh wave are predicted to prevail in microtremors, and H/V to express the ellipsoidal trace. The peak period of H/V is assumed to change with the depth of the Vs=500 - 3500m/s layers. Based on the models in Table 5, five bedrock model patterns were assumed, in which the Vs=500, 700, 1000, 1500 and 3500m/s layers were defined as the respective lowermost layers (Figure 7). We calculated H/V of the Rayleigh wave fundamental mode in each pattern and compared the H/Vs of these Rayleigh waves (H/V-R) and the H/Vs of the microtremors observed at the center of array (H/V-M) (Figure 8). On the basis of this comparison, the relation between the H/V peak period and bedrock depth can be found by investigating the pattern that best fits the peak periods obtained by calculation and the H/V of the microtremors.

The features of this comparison fall into two main classifications: ① (KAR, YNG, JHK, NIK, GNT and SHB) and ② (TTA and TTD).

First, for group ①, clear peaks in the H/V-Rs of four patterns, in which Vs = 500, 700, 100, and 1500m/s layers are the lowest, are shown in the period of 0.5 - 1.0s and these value correspond to the H/V-M peak. The H/V-R of the pattern with the lowermost layer of Vs=3500m/s has two peaks in all the regions except SHB, and the short period peak fits the peak of H/V-M. In the SHB, there is only one H/V-R peak which corresponds to the H/V-M peak.

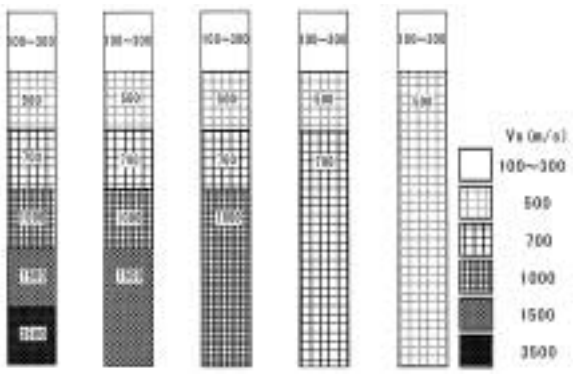

Fig. 7 Subsurface model assumed when the Rayleigh wave fundamental mode is calculated (Figure 9).

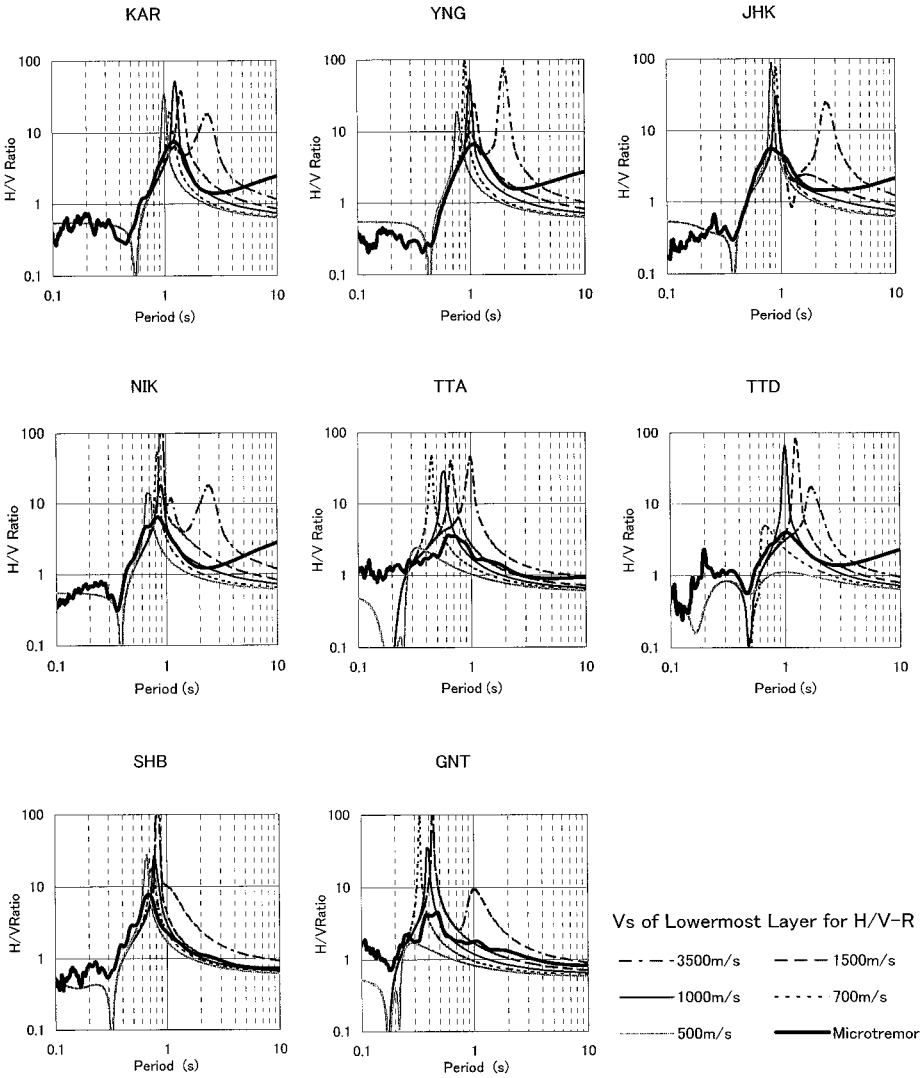

Fig. 8 Comparison of the H/V of the Rayleigh wave fundamental mode (H/V-R) and the H/V of microtremors (H/V-M) at central points of the array sites. We assumed that the lowermost layers are Vs=500, 700, 1000, 1500, 3500m/s layers for the model in the Table 5. Bold solid lines denote H/V-M.

Next, for group ②, H/V-Rs of the four patterns, in which Vs=700, 1000, 1500, and 3500m/s layers are the lowermost, have a clear peak in the period of 0.5s - 1.0s in TTA and in the period of 0.7s - 2.0s in TTD. The H/V-R peak periods of these four patterns differ, those of the Vs=1000m/s and Vs=1500m/s patterns corresponding to the peak period of H/V-M. In this case, the discrepancy of H/V-R and H/V-M peak periods occurs on the short period side in the Vs=700m/s pattern and on the long period side in the Vs=3500m/s one. Accordingly, the case in which the peak period of H/V-R and H/V-M overlap in both groups ① and ② is the Vs=1000 or 1500m/s pattern.

Assuming that the peak period of H/V-M indicates the same bedrock depth in the Tottori plain, the H/V-M peak period corresponds to the bedrock depth to Vs=1000 or 1500m/s layer. In group ① regions, however because the peak period of H/V-R in all the patterns fits the H/V-M peak period, bedrock depth can not be determined from this comparison. A much more detailed investigation is required in order to regard H/V-M as an indication of bedrock depth. Such an investigation is described in Section 6.

Distribution of the peak periods was examined to obtain the relative configuration of the bedrock over the entire plain. A contour map of the peak periods is shown in Figure 9. The 3D bedrock configuration can be roughly obtained from this figure. A shallow bedrock area spreads out over a belt-like zone in the coastal area and bedrock suddenly becomes deep from the eastern mountainous area, including Mt. Kyushou, to the plain around JHK. The deepest area is the basin-like zone around KAR, TTD, YNG, and JHK.

5.3 Determination of the bedrock structure by the Bouguer gravity anomaly

Suitable assumed densities of the surface layers should be used when making a density estimation with the Bouguer anomaly. In this study, the average density of the bedrock was assumed in order to survey the bedrock configuration of the plain. The surface density of the mountainous area around the plain therefore indicates bedrock. In addition, suitable density for the surface layer of the mountainous area around the plain was determined. The

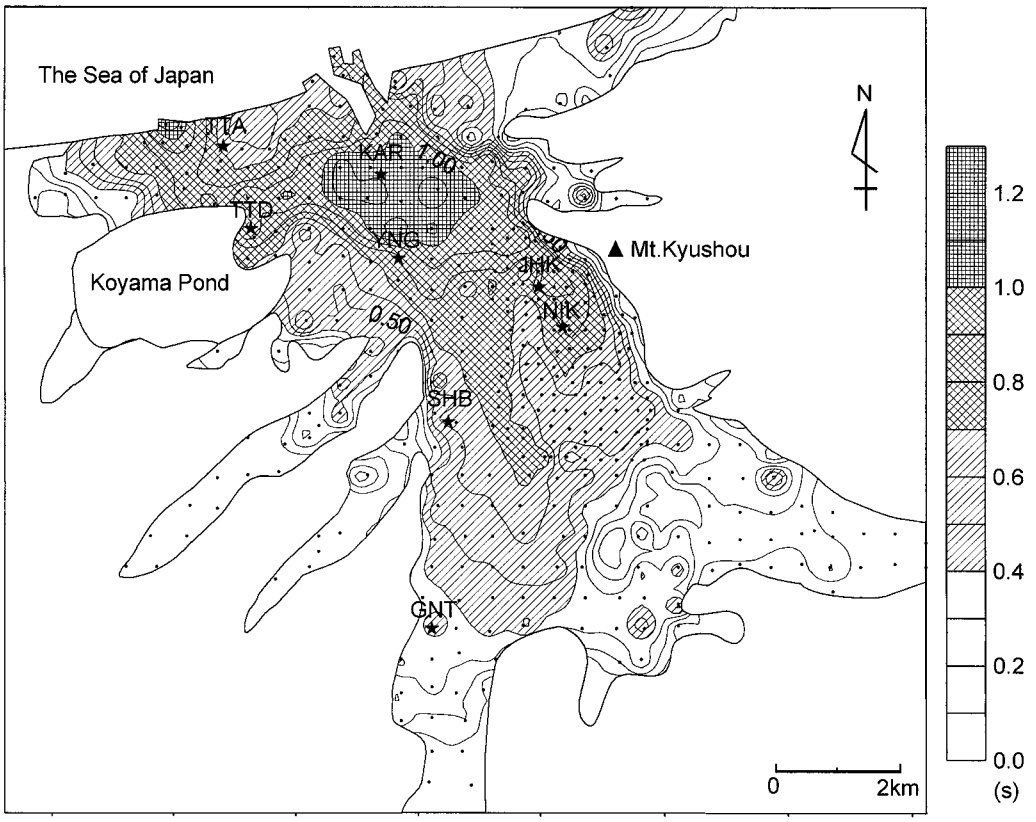

Fig. 9 Contour map of the H/V peak period. The contour interval is 0.1s. Dots shows single-site observation sites, stars array observation sites.

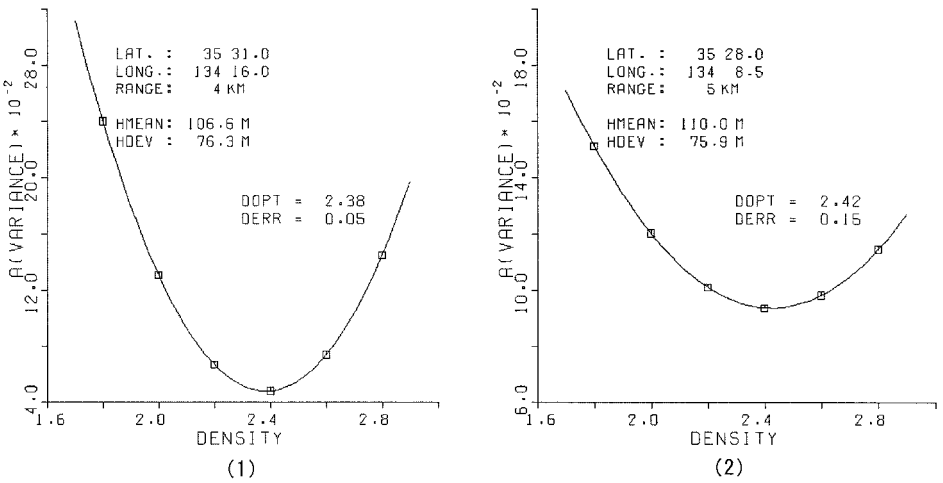

Fig. 10 Density estimations by the CVUR method. Calculated results for (1); the mountainous area of the eastern region and (2); the mountainous area of the western region. The density when the curve takes minimum is the most suitable.

respective calculated density values at two places in east and west were 2.38 and 2.42g/cm^3, which were used for the edge of the plain in a CVUR method (Figure 10). Density measurement results for the rock samples from the east area gives an average dry density for all the samples of 2.59g/cm^3 and an average density for the Neogene system of 2.50g/cm^3 (Table 6) (NEDO, 1977). The Neogene system area is widely distributed throughout the plain (Figure 1). The averaged surface layer density is expected to be less than the value for the rocks because the surface rocks have weathered due to water penetration. As a result, a suitable density for the mountainous area is determined to be 2.50～2.40g/cm^3. The bedrock configuration was determined using a Bouguer anomaly with an assumed density of 2.40g/cm^3.

A filter technique that removes the deep structure effect from the original Bouguer gravity anomaly must be applied to obtain the effect of the subsurface structure. According to Nozaki (1997),

exploration depth is about 1/10 the typical survey line length in the investigation range. Based on Nozaki (1997), exploration depth should be considered to be about 1 km because the objective area is about 10km from south to north. In order to determine subsurface structures shallower than 1 km, band-path filtering was used on the original Bouguer gravity anomaly.

To remove the structure effect of the part deeper than 1km, a band pass filter that combines two upward continuation filters of 50 and 1000m was used. A contour map of the residual Bouguer gravity anomaly is shown in Figure 11. High and low gravity anomaly areas are present near the coast and inland. The gravity anomaly suddenly changes from the mountainous area around Mt. Kyushou to the plain. The low gravity anomaly area is located on the southern side of the plain and the north side of Koyama Pond.

Table 6. Density measurements of rock samples, collected in the mountainous area of the eastern region (NEDO, 1977).

Age		Geology	Number of samples	Density (g/cm^3)			
				Dry Density		Wet Density	
Neogene	Pliocene	Misasa Group	7	2.50		2.53	
	Miocene	Tottori Group	11				
Palaeogene		Intrusive Rocks	16	2.61	2.59	2.63	2.61
Mesozoic		Volcanic Rocks	5				
		Clastic Rocks	3				
Palaeozoic		Weakly Metamorphic Rocks	7	2.75		2.75	

5.4 Quantitave density structure analysis

The density structure was automatically calculated from the observed gravity anomaly. In addition, depth to the bedrock layer in the 2-layer model was restricted to the outcrop point and that of S-wave velocity structural models in the array observation (Table 7). Sections of the 2-dimensional models were set so as not to intersect obliquely with or parallel the anomaly. As gravity anomalies are strongly affected by underlying structures , depth errors in the derived structural models in the area where the 3-dimensional structure effect is large are 10～20% (Komazawa private message).

Table 7. Conditions of control points for analysis of the 2D density structural models. “Distance” means the distance from the left edge in Figure 12. “Depth” means the depth to the Vs=1500m/s layer.

Section	Point	Distance (m)	Depth (m)
A–A'	Rock site	100	0
	Rock site	4100	0
B–B'	KAR	1750	415
	YNG	3050	372
	SHB	5825	195
C–C'	TTD	350	212
	YNG	2700	372
	JHK	5075	485
	Rock site	6300	0

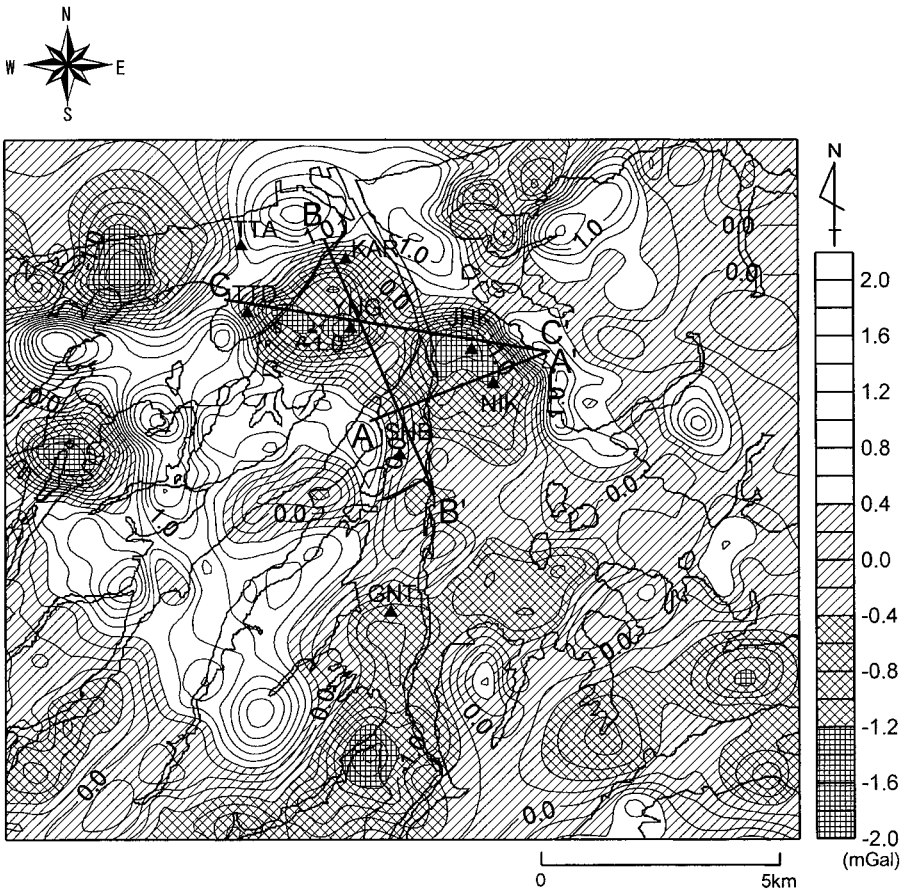

Fig. 11 Contour map of the residual Bouguer anomaly. The contour interval is 0.2mGal, assumed density is 2.4g/cm^3. Band-pass filtering combined two upward-continuation filters, one continued to a height of 50m, the other to 1000m. Triangles show the array observation sites. Lines A-A’ B-B’ and C-C’ mark the location of the 2D density structure model in Figure 12.

First, the A-A' section (Figure 12 (1)) whose both edges are located at outcrop points (border between the mountainous area and a sedimentary layer) was determined. The Society of Exploration Geophysicists of Japan (1988) has reported the relationship between the elastic wave velocity and densities of soils and rocks in each area of Japan. Accordly, the soil density that corresponds to a sedimentary layer of a Vp=1500 - 2000m/s is 1.8 - 2.0g/cm^3, and the soft rock density that corresponds to a Neogene system of Vp=2000 - 3000m/s is 1.9 - 2.1g/cm^3. We consider that the target area should show the same relationship for P-wave velocity and density. The density of the surface layer, including the sedimentary layer and Neogene system, therefore was assumed to be 2.0g/cm^3. The density difference between the surface and bedrock layers was assumed to be 0.4g/cm^3, and the assumed density of the original Bouguer gravity anomaly without filtering was set at 2.4g/cm^3. The upper parts in Figure 12 (1), (2), (3) show the Bouguer gravity anomaly value where the measured and calculated values overlap. The lower parts in Figure 12 (1), (2), (3) give the calculated density structure. According to Figure 12 (1), maximum depth to the bedrock layer is about 350m. The subsurface configuration slopes mildly from the west edge (left side of the figure) to the deepest part, then changing suddenly from the deepest part to the outcrop point.

The B-B' and C-C' section next were determined. These sections are passing through sites the array observation sites where S-wave velocity structure was obtained. In the A-A' section, NIK is the near the deepest part . In the S-wave structural model at NIK, the depth to the Vs=1500m/s layer is the value (358m) nearest the depth for the deepest part of section A-A' (about 350m). These sections were next determined based on the depth to the Vs=1500 m/s layer for the restricted points. Results are shown in Figure 12 (2) and (3). The Bouguer anomaly for the calculated values fits that for the observed one. Accordingly, the density structure model is considered to be the proper one. The B-B' section shows a sudden change from the north edge (left side of the figure) to the deepest part; a mild slope from the deepest part to the center; and a flat configuration from the center to the south edge. The C-C' section shows a flat configuration from the west edge (left side of the

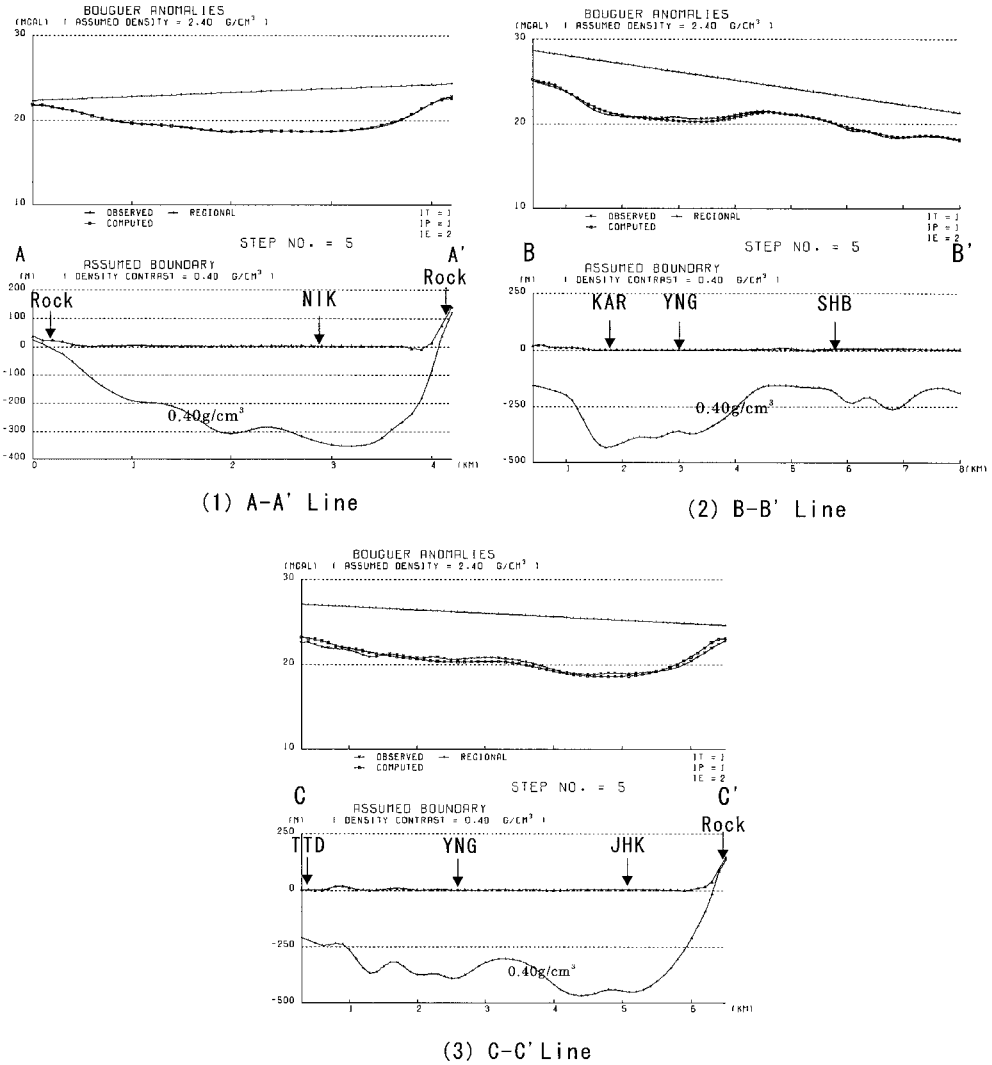

Fig. 12 2D density structure models. The upper part shows the Bouguer anomaly value where the measured and calculated values. Arrows show the locations of the control points in the models. Conditions of the control points of the A-A', B-B', and C-C' sections are shown in Table 7.

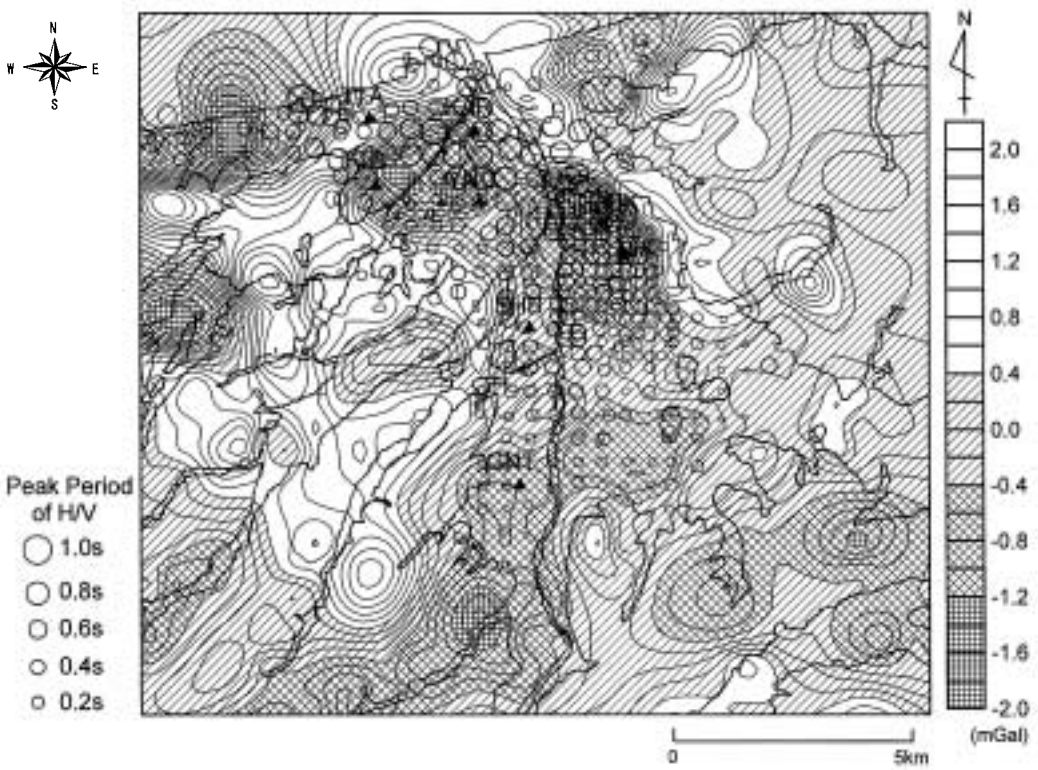

Fig. 13 Overlay map of Figure 9 and 11. Open circles: the H/V peak period. The larger the circle, the longer the period.

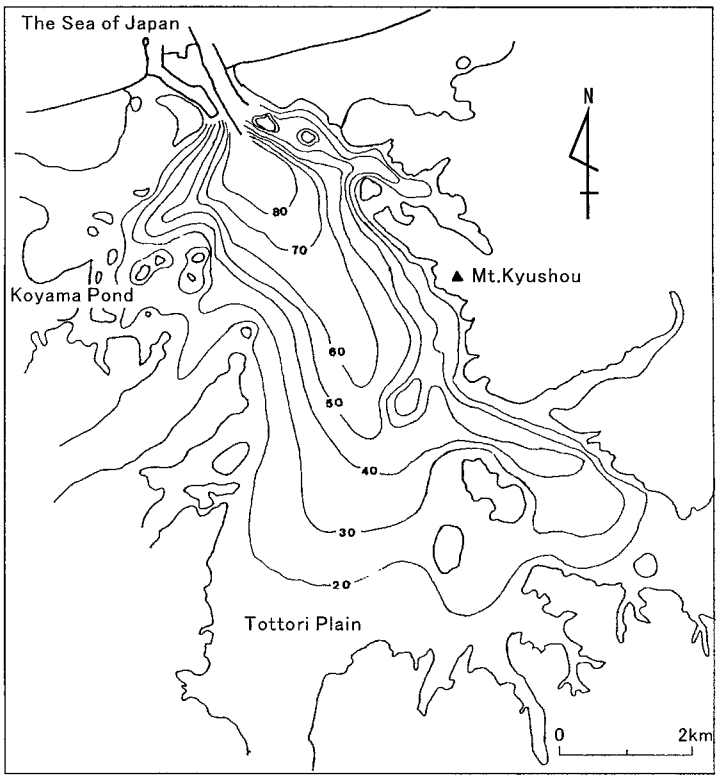

Fig. 14 Contour map of the geological boundary between Quaternary and Neogene in the Tottori Plain (Akagi et al., 1993). The contour interval: 10m.

figure) to the center; a mild slope from the center to the deepest part; and a sudden change from the outcrop points on the subsurface on the east edge to the deepest part.

6. DISCUSSION

First, we reconsider the Rayleigh wave H/V (H/V-R) in TTA and TTD. As stated previously, the peak periods of the Rayleigh wave H/V in the 5 patterns have different values in the ① group (TTA and TTD). In contrast, 4 patterns, except the one having the lowest layer of Vs=3500m/s have almost same values in the other ② group (KAR, YNG, JHK, NIK, GNT, and SHB). We investigated the cause of this difference. Table 5 shows there is a difference between the ① and ② groups for the in Vs=100 - 300m/s layers. The ① group has a thick Vs=300m/s layer whereas the ② group has only a Vs=100 - 200m/s layer. Accordingly, the average velocity value of the layer above the Vs=500m/s layer in the ① group is large, compared with that in ② group; i.e., the velocity contrast between Vs-500m/s layer and upper layers is small in the ① group as compared with that in the ② group. The H/V peak can not be distinguished when the velocity contrast is small (Ohmach et al., 1994). Figure 8 shows that in the ① group, the H/V-R can not be distinguished clearly in the pattern with a lowermost layer of Vs=500m/s, though it is clear in the other patterns. In ② group, however, the pattern having a lowermost layer of Vs=500m/s shows a clear peak as do the other patterns. The velocity structure of the sedimentary layer therefore affects the peak period of the Rayleigh wave H/V.

The peak period distribution of the H/V (Figure 9) was compared with the residual Bouguer gravity anomaly (Figure 11). Two figures are considered to show the 3D relative bedrock configuration. To better visualize this relationship , Figure 9 overlaid with Figure 11 is shown as Figure 13. Open circles in that figure show the H/V peak period. Larger circles represent longer periods. This figure shows that the enlarging tendency of the open circles corresponds to the decreasing tendency of the residual gravity anomalies from SHB to the seashore and from Mt. Kyushou to the plain. These tendencies mean the deepening one of bedrock depth. From SHB to the south side of the plain, the contrary tendency for smaller open circles corresponds to the tendency for a decrease in the residual gravity anomaly. This means that there is a contrary tendency in the south area of the plain on the basis of the bedrock depth. The cause of the low gravity anomaly is thought that bedrock density is not constant, either; bedrock density is low. The geological map in Figure 1 show that the pyroclastics and conglomerates are distributed on the southern side of the mountain area, whereas the granitic and rhyolitic rocks are distributed throughout the area around Koyama Pond and Mt.Kyushou. Those rock densities are lower than the granitic and rhyolitic rock densities, therefore, the southern side is considered to be a low gravity anomaly area because bedrock density is low.

The peak period distribution of H/V (Figure 9) next was compared with findings of a previous study (Akagi et al., 1993). The contour of the geological boundary between the Neogene and Quaternary is shown in Figure 14 (Akagi et al., 1993). The H/V peak period distribution in Figure 9 is the depth distribution from Vs=1000m/s to Vs=1500m/s layer, as stated in 5.2. Figure 14 shows a contour map determined from bore-hole data from the boundary between the sediment and bedrock layers. It is considered to correspond to the depth distribution to the Vs=700m/s layer. This comparison between Figures 9 and 14 is in the strict sense, a comparison of the depth distribution in different layers. Because as the S-wave velocity structure in Figure 6 indicates that the depth change to the Vs=700 m/s layer shows almost the same trend as that to the Vs=1500m/s layer, we believe there is no problem concerning the discussion of relative bedrock depth. Around Mt. Kyushou on the eastern side of the Sendai River and on the coastal area, the sudden change in the configurations of the contour are almost completely overlapped in each figure. Around TTD and TTA northeast part of Koyama pond, there is a the deep area in Figure 9, which it is not shown in Figure 14.

7. CONCLUSION

Microtremor observations and a gravity survey were carried out, and the subsurface structure of the Tottori plain determined. The following conclusions were made:

(1) The array observations of microtremors at 8 sites gave 6 - 8 layers of S-wave velocity structure, the Vs=100 - 3500m/s layers. At the 8 sites, bedrock depths to the Vs=3500m/s layer range from a 300m minimum to an 800m maximum.

(2) Comparison with the calculated H/V-R by used of the structural model suggested that the H/V-M peak period shows bedrock depth from the Vs=1000 to 1500m/s layers, but the relationship between H/V and bedrock depth requires a more thorough investigation.

(3) The 3D bedrock configuration could be roughly determined from the counter maps of the H/V peak period and residual gravity anomaly. The structure where the bedrock suddenly becomes deep along the coast and in the eastern peripheral area of the plain was also determined.

(4) Three bedrock structure cross sections were established based on 2D analysis with the gravity anomaly. In that analysis, a density difference of 0.4g/cm^3 was used, and the bedrock depth to the Vs=1500m/s layer of the S-wave velocity structure were used as the control points. Maximum bedrock depth was found about 400m.

ACKNOWLEDGMENTS

We thank Dr. H. Morikawa, (Tokyo Institute of Technology), Dr. K. Miyakoshi and Dr. B. Zhao, (Geo-Research Institute), and Dr. J. Akamatsu, (Kyoto University) for their helpful advice and assistance. We also are grateful to Dr. M. Komazawa (National Institute of Advanced Industrial science and Technology) who provided the gravity data, analysis program, and helpful guidance.

REFERENCES

Akagi, S., Toyoshima, Y., Yoshitani, A., Okada, S., Michiue, M., Hinokidani, H., Miyakoshi, J., Nishida, R., and Shiozaki, I., 1993. Tottori Hot Spring Maintenance and Investigation Report: topography, geological, magnetic, radioactive, leveling, deeper electrical survey (in Japanese).

Aki, K., 1957. Space and time spectra of stationary stochastic waves with special reference to microtremors, Bull. Earthq. Res. Inst., 35; 415-456.

Architectural Institute of Japan, 1944. The Tottori prefecture earthquake disaster investigation report, Jour. of Architecture and Building Science (in Japanese).

Ishida, H., Nozawa, T., Furuya, S., Tkai, T., Kato, K., and Niwa, M., 1996. Estimation of base rock depth distribution under the Kobe urban Area, Jour. Struc. Constr., AIJ, 485, 63-72 (in Japanese).

Kikuchi, S., 1982. Gravity exploration in the analysis of shallow structures, Geophys. Explor., 35; 6; 1-12 (in Japanese).

Kitsunezaki, C., Goto, N., Kobayashi, Y., Ikawa, T., Horike, M., Saito,T., Kurota, T., Yamane, K., and Okuzumi, K., 1990. Estimation of P- and S- wave velocities in deep soil deposits for evaluating ground vibrations in earthquake, Jour. Natural Disaster Science, 9; 3; 1-17 (in Japanese).

Komazawa, M., 1984. On the quantitative gravimetric analysis in the Houkuroku district, Geophys. Explor., 37-3, 19-30 (in Japanese).

Komazawa, M., 1995. Gravimetric analysis of volcano and its interpretation, Jour. Geod. Soc. Japan, 41; 1; 17-45.

Komazawa, M., Hiroshima, T., Ishihara, T., Murata, Y., Yamazaki, T., Joshima, M., Makino, M., Morijiri, R., Shichi, R., Kishimoto, K., Kikawa, E., and Mishima, M., 2000. Gravity measurements data file of the geological survey of Japan, Gravity CD-ROM of Japan, Digital Geoscience Map P-2, Geological Survey of Japan.

Makino, M., 1997. An improved methods for two-dimensional gravity analysis by using logarithmic function, An application to the Kobe area. Geophys. Explor., 50; 2; 123-131 (in Japanese).

Matsushima, T. and Okada, H., 1990. Determination of deep geological structures under urban sreas using long-period microtremors, Geophys. Explor., 43; 1; 21-23.

Miyakoshi, K., Okada, H., Sasatani, T., Moriya, T., S, Ling., and Saito, S., 1994. Estimation of geological structure under ESG blind prediction test sites in Odawara City by using microtremors, Jour. Seismol. Soc. Japan, 2; 47; 273-285 (in Japanese).

Nakagawa, I., Higashi, T., Takemoto, S., Kobayashi, Y., and Nakagawa, S., 1993. Tottori Hot Spring Maintenance and Investigation Report: Gravity survey and electrical exploration, 3-13 (in Japanese).

NEDO (New Energy and Industrial Technology Development Organization), 1977. Fundamental Research Report of Terrestrial Heat Development: No. 10, Shikano, Matsuzaki II, 7-21 (in Japanese).

Nishida, R., Munetou, W., Nakamura, H., Ueda, T., Nishiyama, H., and Noguchi, T., 2001. Subsurface structure analysis by gravity survey, Reports of the 53th Japan Society of Civil Engineers Chugoku Branch Conference, I-48, 95 (in Japanese).

Nozaki, K., 1997. The Latest Microgravity Survey and its Applications, Oyo Technical Report: No.19, 35-60 (in Japanese).

Ohmachi, T., Konno, K., Endoh, T., and Toshinawa, T., 1994. Refinement and application of an estimation procedure for site natural periods using microtremors, Journal of Structural Mechanics and Earthquake Engineering, 489: I-27, 251-260 (in Japanese).

Okada, H., Matsushima, K., Moriya, T., and Sasatani, T., 1990. An exploration technique using long-period microtremors for eetermination of deep geological structures areas, Geophys. Explor., 43; 6; 402-417 (in Japanese).

Oyo Corporation, 1996. Subsurface Research Report for LNG Satellite Equipment, (in Japanese).

Talwani, M., Wozel, J., and Landisma, M., 1959. Rapid computation for two dimensional bodies with application to mendocino submarine fracture zone, Jour. Geophysical. Res., 64; 49-59.

Tokimatsu, K., Arai, H., and Asaka.Y., 1997. Deep share-wave structure and earthquake ground motion characteristics in Sumiyoshi area, Kobe City, based on microtremor measurements, Jour. Struc. Constr., Architectural Institute of Japan, 491; 37-45 (in Japanese).

Tottori Green Tuff Research Group, 1989. Studies on stratigraphy of Tottori Group, Lower and Middle Miocene strata, distributed in the southeast area of Tottori City, southwest Japan, Association for the Geological Collaboration in Japan Reports, 36; 85-104 (in Japanease).

Tottori Prefecture, 1999. Hot Springs Maintenance Research Report (9): -Tottori Spa , 5-72.

Tottori Subsurface Institue, 1991. Tottori Subsurface Profile Map of the Eastern Region (in Japanese).

Society of Exploration Geophysicists of Japan, 1988. Elastic wave velocity of “soils and rocks”: Measurement and Use, 83-84 (in Japanese).

Yamanaka, H., Furuya, S., Nozawa, T., Sasaki, T., and Takai, T., 1995. Array measurements of long-period microtremors in the Kanto plain, Jour. Struc. Constr. Eng, 478; 99-105 (in Japanese).